ORIGINAL RESEARCH PAPER

Degradation of Benzotriazole from aqueous solutions: A synergistic effect of nano- Fe₂O₃@Alg-TiO₂ on UV/Fe₂O₃@Alg-TiO₂ process

Seyedeh Elahe Badiei Khairabadi[1], Hasan Rahmani [2, 3,]*, Mohammad Bagher Miranzadeh [2, 3], Rouhullah Dehghani [2,3], Fatemeh Atoof [4]

[1]Department of Environmental Health Engineering, Faculty of Health, Kashan University of Medical Science, Kashan, Isfahan, Iran

[2] Department of Environmental Health Engineering, Faculty of Health, Kashan University of Medical Science, Kashan, Isfahan, Iran

[3] Research Center for Social Determinants of Health (SDOH), Kashan University of Medical Sciences, Kashan, Iran

[4] Department of Biostatistics, Faculty of Health, Kashan University of Medical Science, Kashan, Isfahan, Iran

ABSTRACT

In this study, the decomposition of BTA was examined using a photocatalytic process (UV/Fe$_2$O$_3$@Alg-TiO$_2$). The effects of various operational parameters such as the initial pH (3-7-10), catalyst dosage (50, 100, 150 mg/L), BTA initial concentration (15–45 mg/L), UV intensity (2, 4, and 6 watts), and detention time (15,30, and 45 minutes) on the decomposition of BTA in the reactor with Batch conditions and in deionized water, real wastewater (three different matrices saline water, and real raw wastewater after activated sludge and after stabilization ponds) were investigated. SEM, XRD, and FTIR determined the synthesized catalyst's specifications. The results showed that 73.5% of BTA and 30% TOC were removed during the UV/Fe$_2$O$_3$@Alg-TiO$_2$ photocatalytic process at the optimal condition (BTA=30 mg/L, pH = 3, UV = 4 Watt and catalyst dosage =150 mg/L) in deionized water. Also, the efficiency of the process in removing contaminants from the Saline, real raw sewage after activated, and after activated sludge and stabilization ponds were 23%, 47%, and 51%, respectively. The results showed that the toxicity decreased in 200 minutes and if sufficient time is provided to complete the reaction toxicity can be reduced. The results related to the amount of electrical energy consumed showed that considering both the advantages of BTA removal efficiency and energy consumption, the best performance was obtained in optimum conditions.

Keywords: *Benzotriazole, Cross-Linked Alginate Polymer, Fe$_2$O$_3$ Nanoparticles, Photocatalytic Process, Titanium Dioxide Nanoparticles.*

INTRODUCTION

Emerging compounds resulting from human activities have attracted the attention of researchers due to their significant increase in the environment, especially in aquatic solutions[1]. These contaminants cause severe damage to the environment and adversely affect human health and other organisms. BTA is one of the most widely used emerging compounds due to its good performance, the most polluting substance after EDTA in many natural water sources[2]. It is a chemical substance in high volume that has many applications in industry and the family [3]. BTAs are heterocyclic compounds consisting of three nitrogen atoms with the chemical formula $C_6H_5N_3$ with the structure of the base benzene ring in combination with the tetrazole ring (Table 1) [4, 5]. Applications include inhibition of corrosion [6], biocides in leather and paper industries [7],

* Corresponding Authors Email: *hs.rahmani@yahoo.com*

protection of silverware in the dishwasher, as a catalyst in the healing process in the plastics industry [8], used in coolants and hydraulics, and UV stabilizers) The properties of these materials include high polarity, high solubility in water (e.g., 25 g /L at 20 °C), low vapor pressure, and water-ethanol distribution coefficient $\log K_{ow}$ 1.23) [6]. This compound also shows high resistance to chemical and biological degradation[9]. BTA was identified and suspected of being a carcinogen in 2000 by the Health Communication Network (HCN). It was further classified as an emerging pollutant in 2008 by the United States Environmental Protection Agency (EPA) [10]. One of the ways that this substance enters the environment is through human activities. Its remains have been identified in river sediments, seawater, and sewage [11]. Conventional wastewater treatment processes are less effective in removing organic compounds due to their high toxicity and chemical stability [12]. The concentration of BTA in the environment varies in different seasons, and observations have shown that it increases in colder months [13, 14]. Studies on the removal of BTA using membrane bioreactors (removal rate 61%) [15], activated sludge (removal rate 7%) [16], and chlorine (> 10%) [17] reported very low removal efficiencies of these processes. The advanced oxidation process is a non-selective chemical process that produces hydroxyl radicals in situ. These radicals attack the chemical composition. These radicals effectively break down organic compounds into their simpler and often fewer toxic structures. Among the advanced oxidation processes (AOPs), ozonation, O_3/UV, O_3/H_2O_2 and $O_3/H_2O_2/UV$ is hydrogen peroxide-based methods (e.g., H_2O_2/UV, Fenton, Fenton-like, hetero-Fenton, and photo- Fenton), heterogeneous photocatalysis (TiO_2/UV and $TiO_2/H_2O_2/UV$ systems) can be used for oxidative degradation of organic pollutants and conversion to products such as carbon dioxide and water in various environmental fields [18-25]. Several heterogeneous catalysts used in the photocatalysis method include metal oxides (Al_2O_3, MnO_2, CeO_2, and TiO_2), zeolites modified with metals, and metals supported on media such as activated carbon [7, 8].

Alginate-based composites have been investigated as cost-effective and efficient adsorbents for various applications of the removal of heavy metals, industrial paints, pesticides, antibiotics, hormones, air pollutants, and other contaminants in water and wastewater [26, 27]. Sodium alginate (sodium) Sodium salt is an alligenic acid, a polymer with abundant free hydroxyl and free carboxyl groups distributed along the polymer backbone chain. Natural alligenic acid polysaccharides contain carboxyl groups, and due to their unique colloidal properties, they include thickening, stabilization, suspension, film formation, gel production, and emulsion stabilization [28]. Titanium dioxide has been widely used as a concentrated semiconductor photocatalyst with properties such as chemical stability, availability, corrosion resistance, economic properties, and toxicity [11, 29]. Since nanoparticles do not have magnetic properties, their modification by metallic and non-metallic elements has received much attention. Doped TiO_2 nanoparticles have a new property according to the type of impurity, which improves the physical and optoelectronics performance of TiO_2 nanoparticles [30]. Among ion types, iron ions (Fe^{3+}) are considered a suitable source due to having a radius (0.69 A°) similar to Ti^{4+} (0.745 A°), and therefore, the iron ion can easily penetrate the TiO_2 crystal lattice [14, 22, 31]. Also, doping of TiO_2 by an external element and combining TiO_2 with UV sensitizers [32-34]. One of the significant problems of nanocatalysts is the separation from the treated effluent [25, 33, 35, 36]. Alginate is a biopolymer in which the carboxylic groups in its grains help to remove contaminants from the aqueous medium through adsorption [37]. The advantage is that the protection of magnetic carriers increases the photocatalytic activity and increases the lifespan of magnetic photocatalysts[38, 39]. The innovation of this research is the use of sodium alginate as a Fe_2O_3@Alg-TiO_2 nanocomposite cross-linking between Fe_2O_3 as the center of the composite core and TiO_2, and limited studies have been conducted on the use of this compound and that in the synthesis of compounds different from the present study. This study investigated the effect of UV/Fe_2O_3@Alg-TiO_2 on removing BTA from a liquid medium. Novelty and the main purpose of this study were to modify Fe_2O_3 MPNs with cross-link polymer of Fe^{2+}/Fe^{3+} ions for simultaneous use of UV/Fe_2O_3@Alg-TiO_2 process and separation of catalyst from effluent and its prevention into the environment. In addition, the simple advantages of this new catalyst are the simple synthesis, eco-friendliness, cheapness of Fe_2O_3@Alg-TiO_2 nanoparticles, easy separation, and multiple applications of almost complete catalysts.

2

J. Water Environ. Nanotechnol., 9(1): 1-17 Winter 2024

EXPERIMENTAL SECTION

Reagents

1H-BTA (99% purity) was obtained from Sigma-Aldrich, and fresh solutions of BTA (500 mg L^{-1}) were prepared by diluting an appropriate amount of solid reagents with deionized water (DI water).

Methanol HPLC grade, $FeCl_2 \cdot 4H_2O$ $FeCl_3 \cdot 6H_2O$, and sodium alginate were obtained from Sigma Aldrich (USA). Also, ammonia solution ($NH_3 \cdot H_2O$), acetonitrile of gradient grade for liquid chromatography, and titanium (IV) isopropoxide ($C_{12}H_{28}O_4Ti$) were purchased from Merck (Germany).

Preparation and characterization of TiO$_2$

To produce TiO_2 nanoparticles, the hydrothermal method was used microwave-assisted. Two solutions with 0.01 mol $TiOSO_4$ (as precursor solution) and 0.6 mol NaOH (as a mineralizing solution) in deionized water were prepared by continuous stirring. After obtaining a homogeneous solution, the solutions are mixed and stirred continuously until they reach a temperature of 50 °C and pH 14. The resulting solution was transferred to a Teflon reactor and heated under the microwave for 30 minutes at 170 °C. In the final step, the white powder formed in the reaction was washed by centrifugation at room temperature to a neutral pH (~ 7). The powder was then dried in the oven at 60 °C to ensure that the powder was dry (for at least 10 hours).

Catalyst synthesis

First, 1 g of Fe_2O_3 nanoparticles was dispersed in 100 ml of 2.5 g sodium alginate solution, and the mixture was exposed to ultrasonic waves for 30 minutes. Then 0.5 g of titanium Dioxide was added to the mixture. It was again exposed to ultrasonic waves for 30 minutes, and the product was washed four times (with deionized water) and dried in an oven for at least 2 hours. The morphology and structural properties of the produced catalyst were investigated during SEM, XRD, TEM, and FTIR analyses.

Experimental procedure

To prepare the examined concentrations of BTA, the first 500 ppm solution was made, and from the 500 ppm solution, 100 ppm solution was made, which was used to prepare samples with concentrations of 15, 30, and 45 ppm. In the next step, the samples were poured into a reactor made of quartz, and specific doses of catalyst [50, 100, 150 mg/L] were added to the reactor, which was in contact with UV light (with a nominal power of 2, 4, and 6 watts). An ultraviolet lamp was placed near the reactor. In this study, different reaction times were considered for the concentration of each contaminant as well as the catalyst. Reaction times varied from 10, 30, and 50 minutes. Experiments were performed in different environmental conditions at pH = 3, pH = 7, and pH = 11. Inlet and outlet samples of the reactor after preparation (separation of the catalyst using a centrifuge and passing through a filter of 0.2 μm) were transferred to HPLC with Detection Limit values equal to 0.3 mg/L to determine the removal efficiency of BTA [15]. To prepare the calibration curve of the device, first, a solution with specific concentrations of BTA was given to the device to be detected by HPLC, and unknown concentrations were obtained by calculating the area under the peak, which was done by the HPLC device. The amount of BTA removed during the process was then determined by HPLC. After determining the residual concentration of BTA in the samples, the removal efficiency was measured for each of the different conditions, and the optimal reaction conditions were determined.
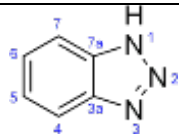
Analytical methods

BTA is immediately equipped with an advanced HPLC device equipped with an ultraviolet detector (KNAUER Smart line UV Detector 2500) at a wavelength of 254 nm and a C_{18} column as a stationary phase of the device with an estimated detection limit of 0.3 mg /L (nominal diagnostic limit) was analyzed. The mobile phase of a methanol/water mixture was 70:30 (v / v). The flow rate was kept at 0.2 ml min^{-1}, and the injection volume was 10 μL in all the samples. To determine the intermediate and final compounds obtained from the BTA and Fe_2O_3@Alg-TiO$_2$ process under optimal conditions, the HP 5975c Agilent, as a chromatography device, made in the USA equipped with the model mass detector (FID) was used.

RSM model

One of the multivariate techniques used in analytical optimization is the response surface methodology (RSM). The aim is to simultaneously optimize the levels of variables for the best system performance. The design of this determination experiment for the optimal chemical and physical

J. Water Environ. Nanotechnol., 9(1): 1-17 Winter 2024

3

Table 1: Physical and chemical properties of Benzotriazole

Molecular Structure	
Molecular formula	C6H5N3
Molar mass	119.12g/mol
Appearance	solid
Density	1.36g/ml
Melting point	100 °C
Boiling point	350°C
Solubility in water	20 gr/L
Acidic (pKa)	8.2
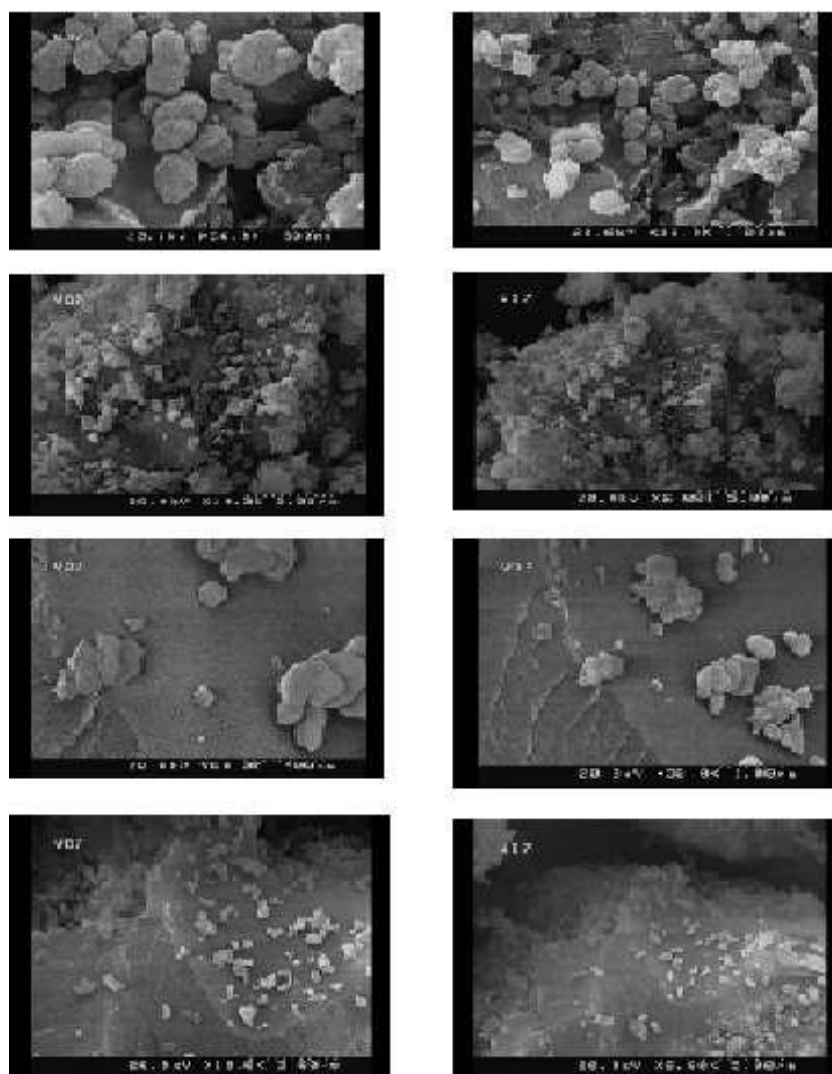
Fig. 1. Scanning electron microscope (SEM) images of Fe_2O_3 @ Alg-TiO$_2$

4

J. Water Environ. Nanotechnol., 9(1): 1-17 Winter 2024

Table 2: Run orders for the three levels of all variables

Run	Factor 1	Factor 2	Factor 3	Factor 4	Factor 5	Response 1	
	A: Time (min)	B: BTZ (ppm)	C: Cata (g/L)	D: UV (Watt)	E: pH	R1 (%)	EE/O
1	10	30	0.1	6	7	44.2	40.46
2	30	30	0.1	4	7	54.1	25.01
3	30	15	0.05	4	7	39	19.73
4	30	30	0.15	4	3	73.5	22.74
5	30	45	0.1	2	7	34	19.16
6	30	30	0.1	4	7	53.5	25.11
7	50	30	0.1	4	11	24.5	34.95
8	30	30	0.1	4	7	53.6	25.10
9	30	45	0.1	4	11	14.5	55.75
10	10	30	0.1	4	11	10	63.46
11	50	30	0.15	4	7	62.1	23.83
12	10	30	0.1	4	3	56.7	24.60
13	30	30	0.1	4	7	51.8	25.41
14	30	45	0.15	4	7	68.9	30.45
15	30	45	0.05	4	7	50.8	33.41
16	30	30	0.05	4	3	50.3	25.68
17	50	45	0.1	4	7	30.1	40.13
18	10	30	0.05	4	7	28.8	32.33
19	30	30	0.1	6	11	22	55.42
20	50	30	0.1	4	3	68.7	23.04
21	30	30	0.15	6	7	61.8	35.81
22	30	45	0.1	6	7	45.1	52.11
23	30	30	0.1	4	7	51.8	25.41
24	50	15	0.1	4	7	59.9	15.87
25	30	30	0.05	4	11	20.3	38.59
26	30	30	0.05	6	7	32.5	45.92
27	50	30	0.05	4	7	46.8	26.39
28	10	30	0.1	2	7	38	14.32
29	30	30	0.1	4	7	54.1	25.01
30	10	45	0.1	4	7	35.5	37.74
31	30	30	0.1	6	3	69.4	34.44
32	30	15	0.1	4	11	30	23.17
33	30	30	0.05	2	7	29.9	15.89
34	30	30	0.15	4	11	26	33.94
35	30	30	0.1	2	3	66.5	11.64
36	30	15	0.1	4	3	65.1	15.29
37	50	30	0.1	6	7	70.6	34.25
38	30	15	0.15	4	7	64.2	15.39
39	30	15	0.1	2	7	56	8.19
40	30	15	0.1	6	7	60.1	23.78
41	30	30	0.15	2	7	60.2	12.04
42	10	15	0.1	4	7	59.8	15.89
43	10	30	0.15	4	7	56	24.71
44	50	30	0.1	2	7	54	12.51
45	30	30	0.1	2	11	15	23.17
46	30	45	0.1	4	3	61	31.57

process is determined as follows [16, 24]. The Box-Behnken method was used to estimate the sample size to save costs by using Design Expert 11 software. By repeating the experiments once more, the sample size required to experiment, taking into account 5 variables, each of which is considered in three levels, is equal to 50. (Table 2)

After collecting and entering the software, the data were analyzed, error-corrected, and then described using descriptive statistics such as central

J. Water Environ. Nanotechnol., 9(1): 1-17 Winter 2024

5

Table 3: Independent variables and their levels of experimental values (lowest and highest selected values).

level			symbol	Independent variables
high (1)	Medium (0)	Low (-1)		
11	7	3	X_1	Initial concentration of pollutants
0.15	0.1	0.05	X_2	Nanoparticle dose
50	30	10	X_3	Retention time
45	30	10	X_4	pH
6	4	2	X_5	UV
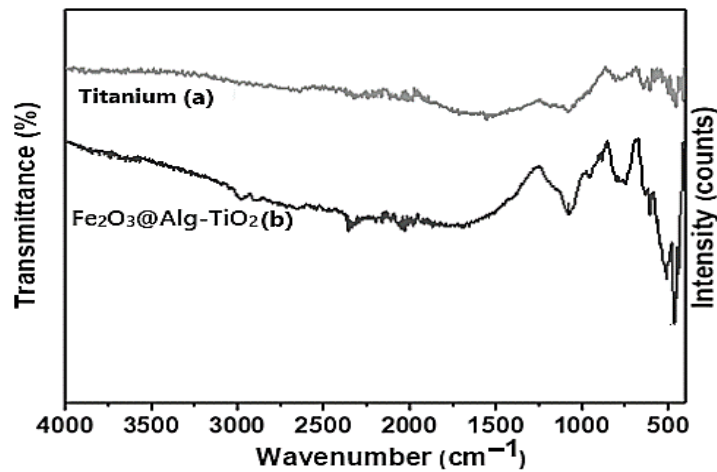
Fig. .2. Synthesized FT-IR spectrum of Fe_2O_3@Alg-TiO_2

indicators, and dispersion of quantitative variables, and the necessary tables and graphs are drawn. For statistical modeling, surface regression was used, considering linear form, quadratic form, and interactions.

$$Y = \beta_O + \sum_{i=1}^{k}\sum_{i=1}^{k}\beta_{ij}x_ix_j + \sum_{i=1}^{k}\beta_{ij}x_{ii}^2 + \varepsilon \qquad \text{(Eq. 1)}$$

For this purpose, the correlation between the response variable of removal percentage ... (y) and five independent variables pH (x_1), time (x_2), pollutant concentration (x_3) and ultraviolet radiation (x_4) and the amount of catalyst (x_5) were examined through surface regression analysis considering the linear form, the quadratic form, and interactions, the equation of which is as follows by default:

y= b0 + b1x1 + b2x2 + b3x3 + b4x4 +b5x5 + b11x12+ b22x22+ b33x32+ b44x42+ b55x52+ b12x1x2 + b13x1x3 + b14x1x4+ b15x1x5 + b23x2x3+ b24x2x4 + b25x2x5+ b34x3x4 + b35x3x5 + b45x4x5 (Equ.2)

In a way that "y" is the predicted response, "b_0" is constant coefficients, b_1, b_2, b_3, b_4, and b_5 are related to linear coefficients, b_{11}, b_{22}, b_{33}, b_{44}, and b_{55} are related to quadratic coefficients and b_{12}... b_{45} are related to interaction coefficients. In this study, the backward method is used to select predictive variables in the model. Residual normality and lack of fit tests were also used to evaluate the appropriate processing of the final model. Also, the values of R^2, R^2adj, and R^2Pre, which indicate the ability of the model to predict the percentage of BTA removal from independent variables, are presented. Finally, the optimal values of each independent variable were obtained using numerical methods. To determine the statistical model proposals for the optimal point, validation was performed in the laboratory with confirmatory experiments with the proposed combinations of the statistical model (Table 3).

RESULTS AND DISCUSSION
Characterization of nano Fe_2O_3@Alg-TiO_2
SEM

The appearance and average diameter of the catalyst particles were obtained with the help of scanning electron microscope (SEM) images. The
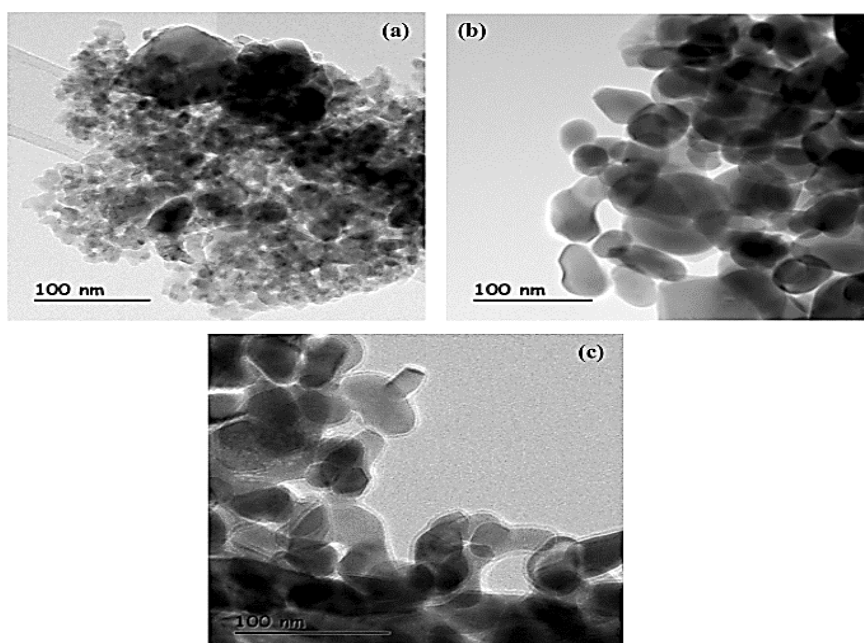
Fig. .3. TEM micrograph of (a) Fe_2O_3, (b) TiO_2, (c) Fe_2O_3@Alg- TiO_2

synthesized samples in this study were imaged by scanning electron microscope or SEM, as shown in Fig. (3). As shown in the pictures, Fe_2O_3@Alg-TiO_2 Nano-catalyst is in the form of aggregates with tiny spherical crystals and particle sizes of 48.7 nm or less.

FTIR

FT-IR analysis is performed to determine the structural properties of Fe_2O_3/TiO_2. Fig. (2a) FT-IR shows the spectrum of Fe_2O_3@Alg-TiO_2 in the wave-count range. Examination of the FT-IR spectrum of the Fe_2O_3@Alg-TiO_2 nano-catalyst in the range of 584 cm^{-1} shows the tensile vibrations associated with the Fe-O bond. The broad bands formed in the 1500 cm^{-1} region are also related to the flexural and tensile vibrations of the OH surface water-adsorbed molecules, indicating the tendency of the surface of iron oxide nanoparticles to the hydroxyl group showing the dependence between the Fe_2O_3 nucleus and TiO_2 shell. This correlation is confirmed in the peak between 470 to 1600 cm^{-1}. According to Waldron, ferrites can be considered crystals with continuous bonds [17]. Atoms are joined by an equal force (ionic force, covalent, or Van der Waals force). The peaks confirm the structure of the spinels and the XRD result. The peak is attributed to the O-H bond and is most likely due to the presence of water [40].

Morphological Studies by Transmission Electron Microscopy

To investigate the structure more closely, nanocomposite samples were characterized by TEM.

Fig. 3 (a-c) is related to the TEM images before and after the synthesis of Fe_2O_3@Alg-TiO_2 nanocomposite. The results of the Fe_2O_3 particle size analysis showed a range between 25 and 35 nm, and the TiO_2 particle size was about 20 nm. Fig. 3c clearly shows the core-shell structure of the Fe_2O_3@Alg-TiO_2 nanocomposite. The approximate diameter of the core is about 40 nm and the thickness of the shell is about 5 nm. Based on TEM images, Fe_2O_3@Alg-TiO_2 nanocomposite samples were successfully synthesized using a simple co-precipitation technique.

XRD

One of the ways to identify the type and composition of materials is the X-ray diffraction (XRD) test. X-ray diffraction (XRD) of the D_8 Advanced Bruker AXS model using a Ka-Cu beam (copper cathode) was used to determine the crystal structure of titanium dioxide nanoparticles as well as its crystalline phase [20].

The results obtained from this test on the studied sample show that the model has a crystalline structure and is of the rutile crystal type. The intensity of the peaks indicates that doping

Table 4: Description of the factors examined in the removal of Benzotriazole.

Factor	Name	Units	Type	Minimum	Maximum	Mean	Std. Dev.
A	Time	(min)	quantitative	10.00	50.00	30.00	11.43
B	BTZ	(ppm)	quantitative	15.00	45.00	30.00	8.57
C	Cata	(g/L)	quantitative	0.0500	0.1500	0.1000	0.0286
D	UV	(Watt)	quantitative	2.00	6.00	4.00	1.14
E	pH	-	quantitative	3.00	11.00	7.00	2.29
R	R1	%	quantitative	12	73.5	45.97	16.31

Table 5: Results of fitting a quadratic model with the backward algorithm to the data set (response variable: Benzotriazole removal percentage)**.**

Source	Sum of Squares	df	Mean Square	F-value	p-value	
Model	11.58	5	2.32	11.22	< 0.0001	significant
Lack of Fit	5.90	20	0.2952	33.32	< 0.0001	Suggested
Pure Error	5.90	20	0.2952			
Cor Total	2298.40	50	45.97			
R^2	0.9299					
Adjusted R^2	0.8816					
Predicted R^2	0.7224					
Adeq Precision	18.62844					

with iron and replacing it with titanium destroys the crystal structure to a point. It is shown in the Fig. (2B). The XRD pattern for the samples of titanium dioxide (No. 1283-084-01) and iron oxide (No. 0597-089-01) corresponds to their standard card, and a slight additional peak (No. 2096-087-01) related to quartz impurities (SiO_2) has been observed. Diffraction peaks confirm the composite structure of Fe_2O_3@Alg-TiO_2 [18, 19]. According to Scherer, if the crystals in a powder are small enough, the maximum diffraction pattern expands by a value commensurate with the crystal size [41]. In the resulting sample, titanium dioxide has a rutile structure, and the existing iron oxide is of hematite type.

Modeling and statistical analysis

The description of the variables examined in this study is summarized in Table (3). As observed, BTA's maximum removal percentage is 73.5% in this study.

The quadratic model was fitted to the data set by the backward algorithm. Table (4) shows the results of fitting the quadratic model with the backward algorithm to the data set. According to the results of this table, the variables of reaction time, catalysts, and BTA significantly affect the percentage of BTA degradation. Also, pH variables significantly affect the degradation rate of BTA both quadratically and through interaction with the UV variable.

According to the results of Table (3–5), the resulting model is significant. Also, the lack of fit test is not significant; leverage values between 0 and 1 and the range of Internally Studentized Residuals are ± 3σ. Also, the Signal-to-noise ratio value (Adequate Precision Ratio) is equal to 6284.18, which is desirable because the number is higher than 4. Also, according to Fig. (3), all the residues are scattered along a straight line, which indicates that the residuals are assumed to be normal. According to the diagram, all the points are well distributed around the bisector line of the first quarter. Predicted R^2 is also equal to 0.7224, which means that 72.24% of the total changes in BTA degradation percentage can be justified through this model.

The model coefficients with a 95% confidence interval are summarized in Table (3A). Therefore, the final fitted model is as follows:

Remove = -3.8634 + 0.0862 Time + 0.1022 BTZ + 96.1643Cata + 0.3137 UV +0.90998121824969 pH + 0.0004 Time * BTZ - 0.4805 Time * Cata - 0.0033 Time * UV + 0.0026 Time * pH + 0.0037 BTZ * UV - 0.010 BTZ * pH - 0.863 Cata * UV -2.7576 Cata * pH + 0.0183 UV * pH - 0.0003 Time ^{2} - 0.0012 BTZ ^{2} - 184.2751 Cata ^{2}- 0.034882

8

J. Water Environ. Nanotechnol., 9(1): 1-17 Winter 2024
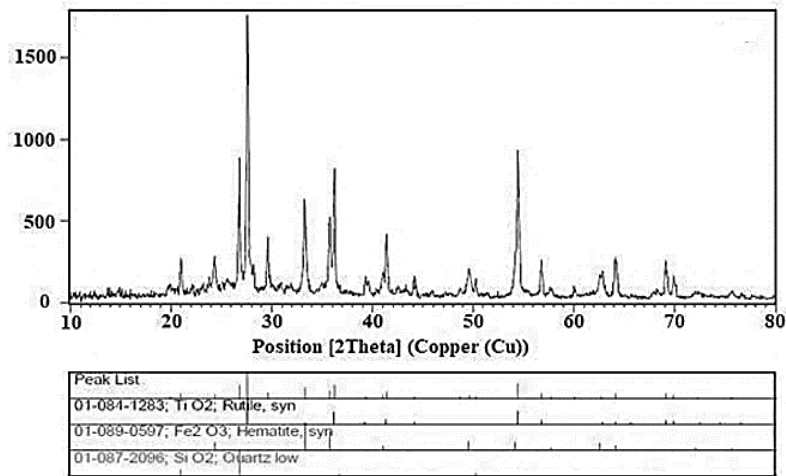
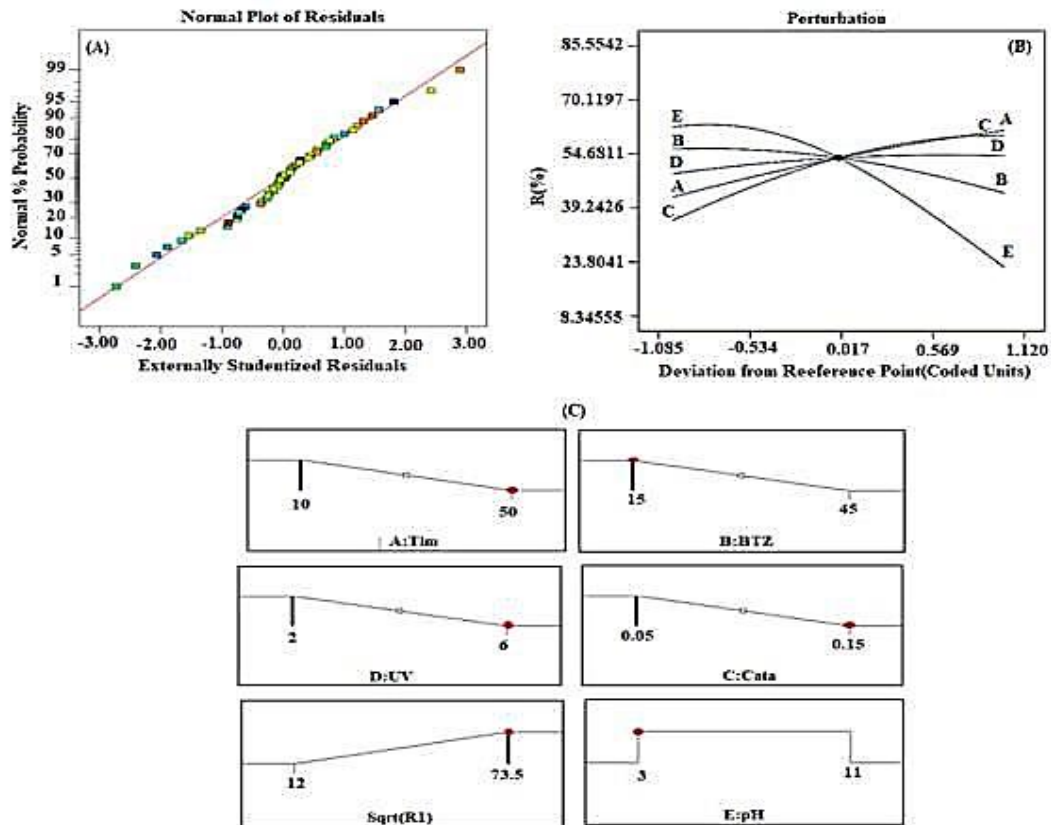Fig. 4. X-ray diffraction pattern of Fe_2O_3@AlgTiO$_2$ photocatalyst

Fig. .5. (A) Displays the normal state of the residues in the fitted model; (B) Chart of turbulence in Benzotriazole removal; (C) Desirability for maximum Benzotriazole removal percentage based on minimum Benzotriazole dose.

$UV^2 - 0.06315$ pH   (Equ. 3)

Estimating model coefficients indicates how independent variables affect BTA degradation percentage; in other words, these coefficients indicate how much BTA degradation percentage is expected to change for each unit of one variable when other variables are kept constant. Negative coefficients show a decrease in the degradation percentage, and positive coefficients show an increase in the degradation percentage.
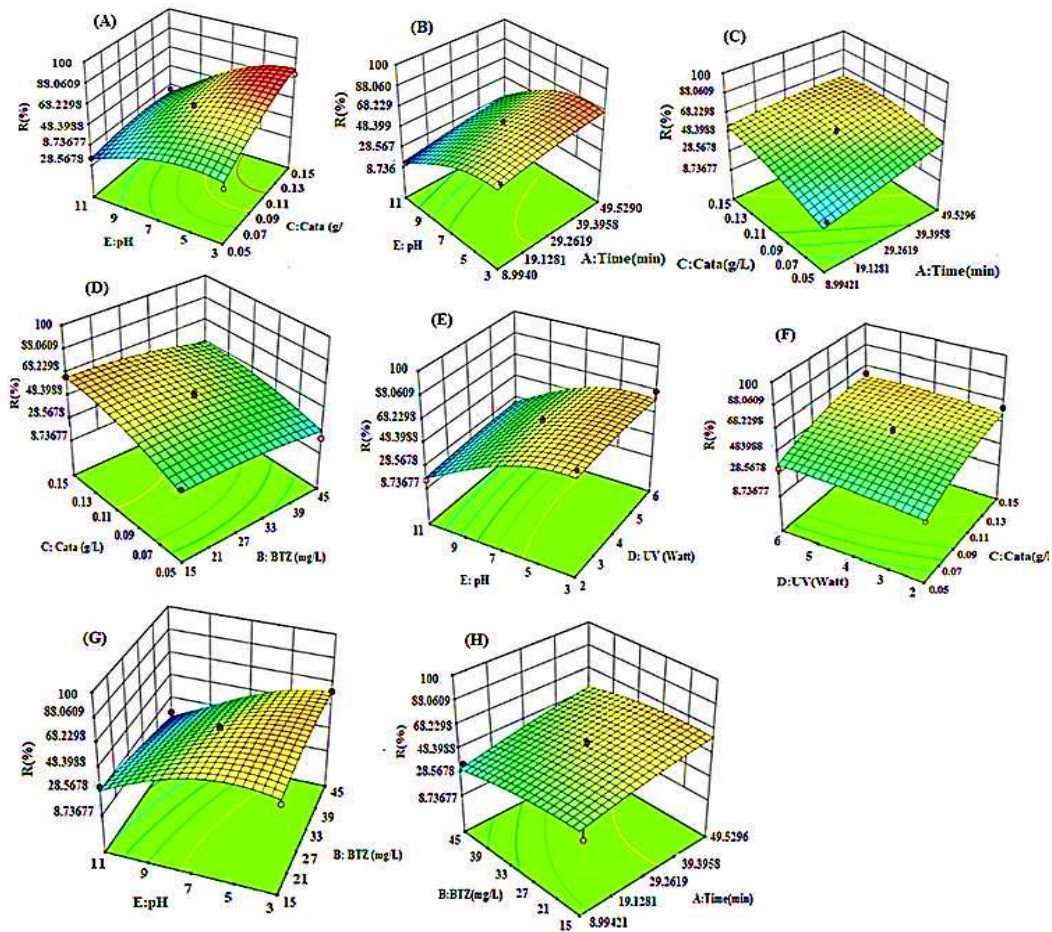
J. Water Environ. Nanotechnol., 9(1): 1-17 Winter 2024

9

Fig. .6. Three-dimensional diagram of response surface based on variables, (A) Cata, pH (Time=30 min, BTZ=30ppm, UV=4), (B) Time and pH (UV=4, BTZ=30ppm, Cata=0.1g/L), (C) Time and Cata (UV=4, BTZ=30ppm, pH=7), (D) Cata and BTZ (UV=4, Time=30min, pH =7), (E) UV and pH (Time=30min, BTZ=30 ppm, Cata=0.1g/L), (F) Cata and UV (pH=7, BTZ=30ppm, Time=30min), (G) BTZ and pH (UV=4, Time=30min, Cata=0.1g/L) and (H) Time and BTZ (UV=4, pH=7, Cata=0.1g/L)

For example, by increasing one unit of BTA the percentage of BTA degradation increases by 75.6% when the other variables are unchanged. According to Fig. (6A), the steep slope obtained from the three factors of BTA and UV and the curvature of the pH factor means that the degradation percentage of BTA is strongly influenced by these factors. Fig. (6 C) shows the optimal value for the maximum percentage of BTA degradation based on the minimum dose of BTA, UV, and pH in the range of 10 minutes and the catalyst dose (0.05) Intended for them) shows. According to the selected criterion, the numerical optimization method obtained the maximum degradation percentage of BTA equal to 73.5% at a dose of BTA equal to 30 mg/L, pH = 3, and UV = 4, and a catalyst dosage of 150 mg/L. Surface Response and Contour Response diagrams in investigating

the effects of independent variables on BTA degradation percentage and considering the existence of significant interactions in the model have been separately shown in Fig. (4). It should be noted that the diagrams are drawn in such a way that the two independent variables are changeable in the coordinate axes, and the other variables are at the optimal point.

Degradation efficiency in the photocatalytic process, as well as in the advanced oxidation processes, is influenced by the operating parameters, including pollutant concentration, pH, UV intensity sources, and the amount of catalyst used and contact time. Therefore, in this project, experiments were performed to obtain optimal values such as catalyst content, pH, BTA concentration, and radiation intensity for the photocatalytic process.

10

J. Water Environ. Nanotechnol., 9(1): 1-17 Winter 2024

The initial concentration of BTA

To investigate the effect of initial BTA concentration on the efficiency of the photocatalytic process at the catalyst dose (0.05, 0.1, and 150 mg/L), the oxidation process with concentrations of 15, 30, and 45 mg/L of the initial concentration of the contaminant was investigated. Removal efficiency decreased with increasing contaminant concentration. Under these conditions, contaminants cover the active sites of the catalyst surface and the contaminant molecules in the area. The effect of UV absorption by contaminating molecules also plays a vital role in reducing the degradation rate. These agents reduce the production of hydroxyl radicals at the catalyst surface [42]. Another factor in reducing the efficiency of the contaminant removal process at higher concentrations could be related to the equilibrium related to the number of active hydroxyl radicals and the number of related pollutant molecules. Due to the process's constant capacity to produce active hydroxyl radicals, more time is required to decompose and remove BTA molecules. Constant first-degree changes were irradiated with a catalyst dose of 50 mg/L and different concentrations of BTA for 30 minutes.
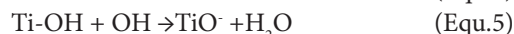
Effect of catalyst on BTA degradation

The amount of catalyst is an essential factor in removing contaminants. The optimal amount of catalyst for BTA degradation by UV/Fe$_2$O$_3$@Alg-TiO$_2$ process was evaluated by adding different catalyst concentrations (0.05, 0.1, 0.15 g /L). As the amount of catalyst increased, so did the removal of contaminants. As the dose of the catalyst increases, the number of active sites on its surface increases. Maximum photon absorption occurs. The efficiency of photocatalytic systems decreases with increasing concentrations above the optimum catalyst point. Although the number of active sites on the surface increases with the amount of catalyst, due to the turbidity created by the catalyst at high concentrations, it reduces the number of active sites on the surface. It increases the light scattering due to turbidity due to high concentrations of catalysts with a concentration of 150 mg/L having the highest percentage of degradation and efficiency [43]. To check the stability and corrosion of the nanocomposite photocatalyst, after the reaction time, the nanocomposite was dried in an oven at 200∘C for three hours and then transferred into a desiccator and cooled down. The results of weighing the nanocomposite after the reaction with an accuracy scale of 1000 did not show any difference in weight compared to before the reaction.

Effect of solution pH on BTA degradation

pH can be effective in material properties and the production of hydroxyl radicals. According to reports, the pH of the solution has a significant effect on the activity of the catalyst, including the particle surface the size of the catalyst in the contaminant structure, and the production of radical hydroxyl [44, 45]. At this stage, the effect of pH on the efficiency of the photocatalytic process and the trend of changes in the percentage of BTA degradation with the reaction time at pH (3, 7, and 11) were investigated. The findings are presented in Fig. (7). Based on these findings, the rate of degradation increased with decreasing pH. The photocatalytic process had the highest efficiency at pH =3. To confirm the results, it is necessary to know that the catalyst has a positive charge at pH =3, and this pH is known as the point charge (PZC) for the catalyst. But at pH> pH$_{pzc}$, the dominant species is TiO$^-$, while at pH> pHpzc, based on the following equations, TiOH^{+2} is the dominant species:

$$\text{Ti-OH + H+} \rightarrow \text{TiOH}^{+2} \qquad \text{(Equ.4)}$$
$$\text{Ti-OH + OH} \rightarrow \text{TiO}^- \text{+H}_2\text{O} \qquad \text{(Equ.5)}$$

According to the above equations, the surface of the catalyst in the acidic medium remains positively charged (pH <7) and negatively charged in the alkaline medium (pH>7). Therefore, the level of TiO$_2$ in an acidic environment has a positive charge, and the adsorption of BTA through nitrogen ions in the structure of BTA is quickly done on the positive level of TiO$_2$ at acidic pH. In a similar study on the photocatalytic degradation of benzene, alkaline sulfonate LAS using linear TiO$_2$ nanoparticles at acidic pH, the degradation rate was faster than the neutral and base pH, and complete degradation (LAS) occurred in less time[34, 45]. On the other hand, the levels of both BTA and catalyst are negatively charged under alkaline conditions, so there is an electrostatic repulsion between the two compounds. Also, in alkaline conditions, the catalyst particles are more prone to shrinkage, which reduces the active surface and the specific surface area of the catalyst per unit area and reduces the production of active radicals, especially active hydroxyl radicals. Therefore, pH =3 was chosen as the optimal pH for BTA degradation due to more hydroxyl radicals in the photocatalytic process.
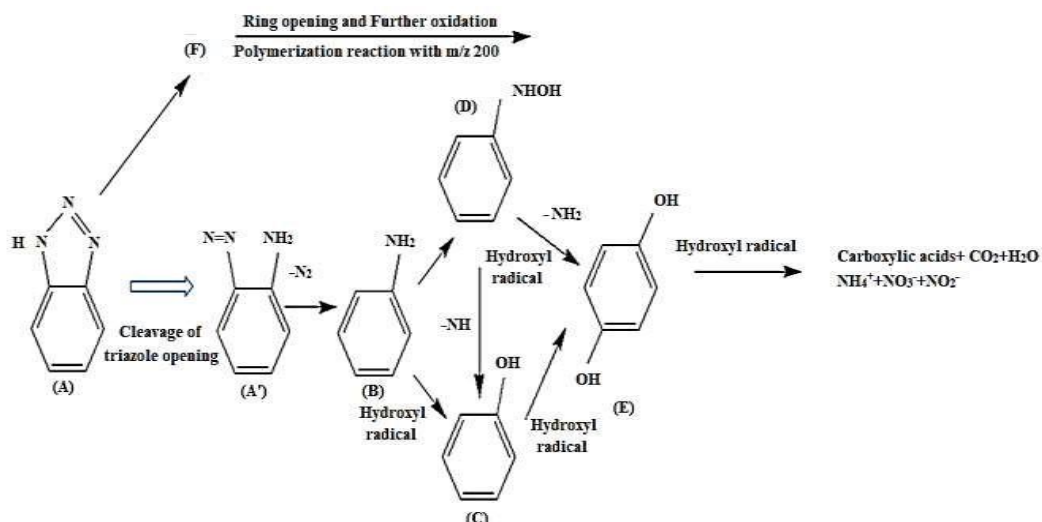
J. Water Environ. Nanotechnol., 9(1): 1-17 Winter 2024

11

Fig. .7. Prediction mechanism for BTA degradation under optimum conditions (Time=30min, BTZ=30 ppm, Cata=0.15g/L, and UV=4W)

Effect of radiation intensity on BTA degradation

The photocatalytic reaction rate largely depends on the absorption of photocatalytic radiation [46]. To investigate the effect of different radiation sources on process efficiency, experiments were conducted with BTA values of (15, 30, and 45 mg/l) and catalyst values of (0.05, 0.1, 0.15 g / L) at pH of (3, 7, and 11) using different sources ultraviolet radiation (2, 4 and 6 watts. Figs. (4E and 4 F), 6-watt bulbs have the highest degradation percentage in BTA degradation due to their wavelength of 254 nm and light intensity of I=25.64 μw/cm². Because, with increasing lamp power (radiation intensity), the excitation rate of the photocatalytic reaction and the formation of electron-hole pairs on the surface of the catalyst, which is strongly dependent on the light intensity, increases. Therefore, it can oxidize organic pollutants [47]. However, at the lower powers of ultraviolet light (2 and 4 watts), the ability to remove BTA is also acceptable.

Mineralization of BTA (degradation pathway)

The mineralization of BTA was studied under optimal conditions by determining the TOC changes. The results showed that the degradation of 30% TOC in 30 mg /L BTA and the catalyst were 150 mg/L at pH 3 and 6 watts of ultraviolet light. The results showed that we needed more time (90 minutes) to convert BTA to the final product. The GC-Mass results show that it is the first intermediate in the degradation of BTA with m/z 120 in the first stage by separating the N = N bond from diazine, from (A′), and aniline (B, m/z=93), benzene ring,

and thiazole ring (disoyimin production) [21].

Aniline and phenazine were reported as major degradation products of BTA [21]. Aniline was further converted to phenol (C, m/z=94) and phenylhydroxylamine (D, m/z=102) in further contact with hydroxyl radicals. Elamine forms hydroquinone (E, 110 m/z) upon loss of NH_2 and contact with free radicals. At this stage, nitrate and nitrite ions are formed by the evolution of nitrogen ammonium ions mineralization. Simultaneously, phenol is formed by contact with oxidized free radicals and hydroquinone as the final aromatic mediator. By opening the benzene ring, carboxylic acids are formed in short chains. Continued oxidation leads to the mineralization of organic compounds and carbon dioxide, water, and mineral nitrogen. The results show that carbon and nitrogen mineralization and further oxidation lead to ring-opening and the mineralization of organic compounds [48].

Application of UV/Fe₂O₃@Alg-TiO₂ photocatalytic process for BTA degradation in real wastewater

The photocatalytic mechanism and charge transfer of the Fe_2O_3-TiO_2 catalyst have been discussed by several authors (Table 6).

At this stage, the photocatalytic efficiency of UV/Fe₂O₃@Alg-TiO₂ for BTA degradation in real wastewater was investigated (three different matrices were selected). Saline water (TOC=20 mg/L, TDS=30000 mg/L, and pH=6.9) and real raw sewage along with secondary effluent from a wastewater treatment plant after activated

Table 6: Summary of existing research on the employment of Fe2O3-TiO2-based nanocomposites photocatalysis for the degradation of POPs.

Pollutant	Catalyst	Irradiation source/time	Operating conditions	Findings	Ref.
2,4- dichlorophenoxyacetic (2,4-D)	Fe_2O_3-TiO_2	6 W UV-A lamp,365 nm	[Catalyst] = 0.2, 0.6,1 [2,4-D] = 10, 30, 50 pH = 4, 7.5, 11	Optimum degradation of 48.64% was obtained with 1.0 g of catalyst, 10 ppm 2,4-D concentration, and at pH 4. Nanocomposite remained stable through the fifth cycle.	(49)
4-chlorophenol	Fe_2O_3-TiO_2	UV lamp (16 W,254–365 nm) 300 W visible light iodine tungsten lamp	[Catalyst] = 2 g [MB] = 25 mg/L pH = 4, 6.28, 9	Nanocomposites calcinated at 880 ∘C exhibited best catalytic activity. MB degradation of 83% and 88% was obtained under UV and visible light, respectively. MB degradation in the third cycle reached 67% and 78% for UV and visible light.	(50)
Acetaminophen (ACT), antipyrine, caffeine, metoprolol, and bisphenol A	Fe_2O_3-TiO_2	TiO_2-Fe_2O_3 TiO_2-SiO_2- Fe_2O_3	Mercury lamp (254 nm), intensity = 3.8 × 10^{-6} einstein L^{-1} S^{-1}	Both photocatalyst exhibited good magnetic properties with saturation magnetization around 40 emu/g The presence of SiO_2 layer restricted the photodissolution of iron.	(51)
non-biodegradable cefixime	Fe_2O_3-TiO_2	power (50–90 W) of ultrasonic waves	catalyst dose = 0.005 g/l, CFX concentration = 15 mg/l, pH = natural (4.5–4.7)	Maximum cefixime degradation (98.8%) occurred at optimum conditions (cefixime concentration = 20.5 mg/L, pH = 4.76, Irradiation time = 103 min and catalyst dose = 0.012 g/l).	(52)

sludge (COD= 300 mg/L, TDS=122 mg/L, and pH=7.85) and along with secondary effluent from a wastewater treatment plant after activated sludge and stabilization ponds (COD=200, TDS=101 mg/L, and pH=8.22) were used for BTA degradation. After centrifugation at 3000 rpm and passing through a 0.2-micron filter, the samples were evaluated under optimal reaction conditions. Then 30 mg/L BTA was added to the solution. As shown in Fig. 6, BTA degradation was reduced in saline water compared to deionized water and secondary effluent. This is due to the higher mineral

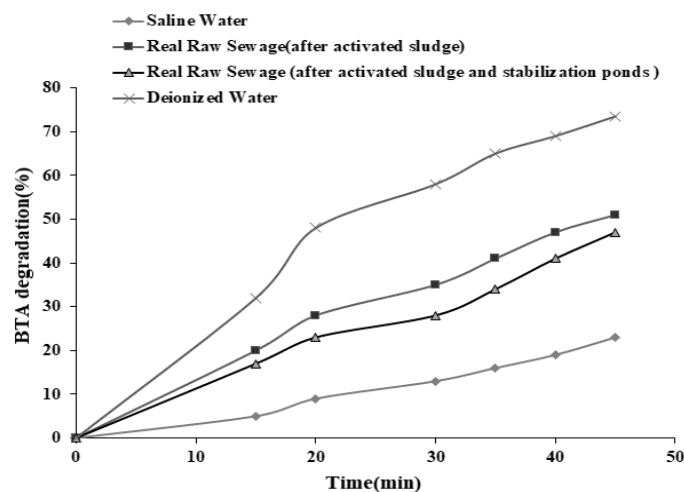*J. Water Environ. Nanotechnol., 9(1): 1-17 Winter 2024*

13

Fig. .8. BTA degradation in different aquatic environments (Time=30min, BTZ=30 ppm, Cata=0.15g/L, and UV=4W)

Table 7: Electrical energy consumption at the ultraviolet lamp.

Run	A: Time (min)	B: BTZ (ppm)	C: Cata (g/L)	D: UV (Watt)	E: pH	R1 (%)	EE/O
4	30	30	0.15	4	3	73.5	22.74
14	30	45	0.15	4	7	68.9	30.45
37	50	30	0.1	6	7	70.6	34.25
39	30	15	0.1	2	7	56	8.19

compositions in the wastewater (various anions).

The reason for reducing the efficiency of the combined UV/Fe$_2$O$_3$@Alg-TiO$_2$ process in real wastewater is the high COD, in which the active radicals produced are spent on other species, in addition to BTA. Investigating the degradation process of BTA in different matrices showed that inorganic compounds (especially anions) have more inhibitory effects than organic compounds. However, the degradation efficiency of BTA in different real wastewater showed that the UV/Fe$_2$O$_3$@Alg-TiO$_2$ process could degrade BTA even in the complex if enough time is provided to complete the reactions.

Electrical energy consumption

As stated below, the amount of electrical energy consumed by the UV lamp to remove BTA in each test period was obtained from the following equation.

$$EE/O = \frac{P \times (t/3600) \times 3785}{V \times \log(C_0/C)}$$
(Equ.6)

That P: lamp power (kW); t: reaction time(s);

V: reactor volume (L); C$_0$: initial concentration of BTA before contact; and C: concentration of BTA after exposure. The results related to the amount of electrical energy consumed during the photocatalytic process are given in Table 5. The results showed that, considering both the advantages of BTA degradation efficiency and energy consumption, the best performance was obtained in run 4.

The effective parameters in calculating the energy consumption are the power of the UV lamp, the contact time, the reactor's volume, and the precursor's initial concentration before and after the process. Since the integration process in optimal conditions caused the degradation of more BTA (73.5%); therefore, this issue increased the system's efficiency due to the energy consumed by a UV lamp.

Toxicity testing during UV / Fe$_2$O$_3$-Alg @ TiO$_2$ process

Microtox analysis was used to evaluate the toxic profiles of BTA during the UV/Fe$_2$O$_3$@ Alg-TiO$_2$ process. The toxicities of untreated and treated samples were tested using a Microtox

14

J. Water Environ. Nanotechnol., 9(1): 1-17 Winter 2024

Model 500 Toxicity Analyzer (Modern Water, Inc., New Castle, DE, USA). In the Microtox test, the luminescent bacteria (*Aliivibrio fischeri*) are used. Untreated and untreated samples were prepared, and activated *Aliivibrio fischeri* was exposed to the samples for 15 minutes, and the toxic units (TU) of each sample were calculated as EC_{50} (%). Due to the inhibition of bioluminescence less than 10% in raw water (100%), the value of TU was considered zero. The results showed that the TU index and toxicity decreased over 50 minutes of BTA exposure in the UV/ Fe_2O_3@Alg-TiO$_2$ process. To study more closely the effect of by-products on the process of wastewater toxicity, the prototype was also exposed to 100 minutes and 200 minutes of the process. The results showed that the toxicity increased in 60 minutes. This was while the toxicity decreased in 200 minutes. According to previous studies, the cause of the increase in toxicity at 100 min can be attributed to the production of by-products during BTA degradation. The decrease in toxicity values over 200 minutes indicates that as the by-products decompose, the TU values decrease. These results indicate that if sufficient time is provided to complete the reaction, BTA can be effectively removed by the UV/Fe_2O_3@Alg-TiO$_2$ process, and the toxicity can be reduced.

CONCLUSION

This study aimed to determine the efficiency of the UV/Fe_2O_3@Alg-TiO$_2$ photocatalytic integrated process in removing BTA from aqueous solutions. The effects of various operational variables such as initial solution pH (3-7-10), specific dosage amount of catalyst (50, 100, 150 mg/L), initial concentration of BTA (15–45 mg/L), the ultraviolet intensity of 2, 4, and 6 watts, and different times (15-30-45 minutes) on the decomposition of BTA in the reactor with Batch conditions were investigated. The results showed that 73.5% BTA was removed during the UV/Fe_2O_3@Alg-TiO$_2$ photocatalytic process at the initial concentration of BTA (30 mg/L), the ultraviolet light intensity of 4 Watt, and under optimal conditions. The results showed that ultraviolet light is essential for the photocatalytic oxidation of organic pollutants. Experiments with radical adsorbents also showed that hydroxyl radical is the predominant oxidizing agent in UV/Fe_2O_3@Alg-TiO$_2$, leading to high mineralization of BTA in solution. Intermediate by-products were identified during BTA degradation. The results also showed that UV/Fe_2O_3@Alg-TiO$_2$

was more effective than the single BTA degradation process in which the role of ultraviolet light was prominent. The efficiency of UV/Fe_2O_3@Alg-TiO$_2$ in real effluent was acceptable due to the high concentration of anions and cations (except in saline water). The results of the Microtox test during the UV/Fe_2O_3@Alg-TiO$_2$ process showed that the toxicity increased in 100 minutes and decreased in 200 minutes. Finally, it can be concluded that if enough reaction time (more than 200 minutes) is provided, the UV/Fe_2O_3@Alg-TiO$_2$ process can be an efficient process for BTA degradation.

CONFLICT OF INTEREST

The authors hereby declare that there is no conflict of interest.

REFERENCES

1. Khan S, Naushad M, Govarthanan M, Iqbal J, Alfadul SM. Emerging contaminants of high concern for the environment: Current trends and future research. Environmental Research. 2022;207:112609. https://doi.org/10.1016/j.envres.2021.112609
2. Wu L, Zhao X, Bi E. Predicting the effect of dissolved humic acid on sorption of benzotriazole to biochar. Biochar. 2022;4(1):15. https://doi.org/10.1007/s42773-022-00134-5
3. Fent K, Chew G, Li J, Gomez E. Benzotriazole UV-stabilizers and benzotriazole: Antiandrogenic activity in vitro and activation of aryl hydrocarbon receptor pathway in zebrafish eleuthero-embryos. Science of the Total Environment. 2014;482:125-36. https://doi.org/10.1016/j.scitotenv.2014.02.109
4. Kraševec I, Prosen H. Solid-phase extraction of polar benzotriazoles as environmental pollutants: A review. Molecules. 2018;23(10):2501. https://doi.org/10.3390/molecules23102501
5. Kowalska K, Felis E, Sochacki A, Bajkacz S. Removal and transformation pathways of benzothiazole and benzotriazole in membrane bioreactors treating synthetic municipal wastewater. Chemosphere. 2019;227:162-71. https://doi.org/10.1016/j.chemosphere.2019.04.037
6. Ahmadi M, Rahmani K, Rahmani A, Rahmani H. Removal of benzotriazole by Photo-Fenton like process using nano zero-valent iron: response surface methodology with a Box-Behnken design. Polish Journal of Chemical Technology. 2017;19(1):104--12. https://doi.org/10.1515/pjct-2017-0015
7. Wang Y, Xie Y, Sun H, Xiao J, Cao H, Wang S. Efficient catalytic ozonation over reduced graphene oxide for p-hydroxylbenzoic acid (PHBA) destruction: active site and mechanism. ACS Appl Mater Interfaces. 2016;8(15):9710-20. https://doi.org/10.1021/acsami.6b01175
8. Yazdanbakhsh A, Rahmani A, Massoudinejad M, Jafari M, Dashtdar M. Accelerating the solar disinfection process of water using modified compound parabolic concentrators (CPCs) mirror. Desalination Water Treat. 2016;57(50):23719-27. https://doi.org/10.1080/19443994.2016.1138147
9. Qin Y, Jiang Z, Guo Y, Mushtaq MA, Shen Z, Du W, et al.

J. Water Environ. Nanotechnol., 9(1): 1-17 Winter 2024

15

Benzotriazole-based structure in porous organic polymer enhancing O2 activation for high-efficient degradation of tetracycline under visible light. Chem Eng J. 2023:141810. https://doi.org/10.1016/j.cej.2023.141810

10. Akkaraju H, Tatia R, Mane SS, Khade AB, Dengale SJ. A comprehensive review of sources of nitrosamine contamination of pharmaceutical substances and products. Regulatory Toxicology and Pharmacology. 2023:105355. https://doi.org/10.1016/j.yrtph.2023.105355

11. Wang S, Zhou S. Titania deposited on soft magnetic activated carbon as a magnetically separable photocatalyst with enhanced activity. Appl Surf Sci. 2010;256(21):6191-8. https://doi.org/10.1016/j.apsusc.2010.03.139

12. Jorfi S, Kakavandi B, Motlagh HR, Ahmadi M, Jaafarzadeh N. A novel combination of oxidative degradation for benzotriazole removal using TiO2 loaded on FeIIFe2IIIO4@ C as an efficient activator of peroxymonosulfate. Appl Catal B. 2017;219:216-30. https://doi.org/10.1016/j.apcatb.2017.07.035

13. Chenari HM, Seibel C, Hauschild D, Reinert F, Abdollahian H. Titanium dioxide nanoparticles: synthesis, x-ray line analysis and chemical composition study. Materials Research. 2016;19:1319-23. https://doi.org/10.1590/1980-5373-mr-2016-0288

14. Sathishkumar P, Anandan S, Maruthamuthu P, Swaminathan T, Zhou M, Ashokkumar M. Synthesis of Fe3+ doped TiO2 photocatalysts for the visible assisted degradation of an azo dye. Colloids Surf A Physicochem Eng Asp. 2011;375(1-3):231-6. https://doi.org/10.1016/j.colsurfa.2010.12.022

15. Wang X, Zhuo N, Fu C, Tian Z, Li H, Zhang J, et al. Enhanced selective adsorption of benzotriazole onto nanosized zeolitic imidazolate frameworks confined in polystyrene anion exchanger. Chem Eng J. 2017;328:816-24. https://doi.org/10.1016/j.cej.2017.07.095

16. Bezerra MA, Santelli RE, Oliveira EP, Villar LS, Escaleira LA. Response surface methodology (RSM) as a tool for optimization in analytical chemistry. Talanta. 2008;76(5):965-77. https://doi.org/10.1016/j.talanta.2008.05.019

17. Waldron R. Infrared spectra of ferrites. Physical review. 1955;99(6):1727. https://doi.org/10.1103/PhysRev.99.1727

18. Aliramaji S, Zamanian A, Sohrabijam Z. Characterization and synthesis of magnetite nanoparticles by innovative sonochemical method. Procedia Materials Science. 2015;11:265-9. https://doi.org/10.1016/j.mspro.2015.11.022

19. Goldstein JI, Newbury DE, Michael JR, Ritchie NW, Scott JHJ, Joy DC. Scanning electron microscopy and X-ray microanalysis: Springer; 2017. https://doi.org/10.1007/978-1-4939-6676-9

20. Khan H, Berk D. Synthesis, physicochemical properties and visible light photocatalytic studies of molybdenum, iron and vanadium doped titanium dioxide. Reaction Kinetics, Mechanisms and Catalysis. 2014;111(1):393-414. https://doi.org/10.1007/s11144-013-0637-3

21. Weidauer C, Davis C, Raeke J, Seiwert B, Reemtsma T. Sunlight photolysis of benzotriazoles-Identification of transformation products and pathways. Chemosphere. 2016;154:416-24. https://doi.org/10.1016/j.chemosphere.2016.03.090

22. R S, N. L. S, E SE, L RD, S MS. An experimental study on photocatalytic degradation to free river water from toxic dye pollutant using Zn doped TiO2 nanoparticles. Journal of Water and Environmental Nanotechnology. 2023;8(3):206-14.

23. Mahmoodi V, Bastami TR, Ahmadpour A. Solar energy harvesting by magnetic-semiconductor nanoheterostructure in water treatment technology. Environmental Science and Pollution Research. 2018;25:8268-85. https://doi.org/10.1007/s11356-018-1224-y

24. Aref S. Employing Sono-Fenton Process for Degradation of 2-Nitrophenol in Aqueous Environment Using Box-Behnken Design Method and Kinetic Study. Russian Journal of Physical Chemistry A. 2019;93(2):243-9. https://doi.org/10.1134/S003602441902002X

25. Rasouli H, Jafarpisheh F, Ghorbanpour M. Synthesis and characterization of Sn-doped TiO2 nanoparticles and the evaluation of their Photocatalytic performance under Vis-lights. Journal of Water and Environmental Nanotechnology. 2022;7(4):344-50.

26. Wang B, Wan Y, Zheng Y, Lee X, Liu T, Yu Z, et al. Alginate-based composites for environmental applications: a critical review. Crit Rev Environ Sci Technol. 2019;49(4):318-56. https://doi.org/10.1080/10643389.2018.1547621

27. Alvani V, Nabizadeh R, Ansarizadeh M, Mahvi AH, Rahmani H. Predicting TOC removal efficiency in hybrid biological aerated filter using artificial neural network. Desalination Water Treat. 2016;57(43):20283-91. https://doi.org/10.1080/19443994.2015.1112839

28. Rhim J-W. Physical and mechanical properties of water resistant sodium alginate films. LWT-Food science and technology. 2004;37(3):323-30. https://doi.org/10.1016/j.lwt.2003.09.008

29. Lv Q, Li G, Sun H, Kong L, Lu H, Gao X. Preparation of magnetic core/shell structured γ-Fe2O3@ Ti-tmSiO2 and its application for the adsorption and degradation of dyes. Microporous and mesoporous materials. 2014;186:7-13. https://doi.org/10.1016/j.micromeso.2013.11.028

30. Chenari HM, Seibel C, Hauschild D, Reinert F, Abdollahian H. Titanium dioxide nanoparticles: synthesis, x-ray line analysis and chemical composition study. Mater Res. 2016;19(6):1319-23. https://doi.org/10.1590/1980-5373-mr-2016-0288

31. Rostami M, Mazaheri H, Hassani Joshaghani A, Shokri A. Using Experimental Design to Optimize the Photo-degradation of P-Nitro Toluene by Nano-TiO2 in Synthetic Wastewater. International Journal of Engineering. 2019;32(8):1074-81. https://doi.org/10.5829/ije.2019.32.08b.03

32. Arora I, Chawla H, Chandra A, Sagadevan S, Garg S. Advances in the strategies for enhancing the photocatalytic activity of TiO2: Conversion from UV-light active to visible-light active photocatalyst. Inorg Chem Commun. 2022:109700. https://doi.org/10.1016/j.inoche.2022.109700

33. Arjmandi P, Hargalani F. Decomposition of petroleum contaminants (naphthol) by ultraviolet (UV) radiation using a green-synthetized titanium dioxide (TiO₂) catalyst. Journal of Water and Environmental Nanotechnology. 2020;5(1):45-55.

34. Helmy ET, El Nemr A, Mousa M, Arafa E, Eldafrawy S. Photocatalytic degradation of organic dyes pollutants in the industrial textile wastewater by using synthesized TiO2, C-doped TiO2, S-doped TiO2 and C,S co-doped TiO2 nanoparticles. Journal of Water and Environmental Nanotechnology. 2018;3(2):116-27.

35. Sharma V, Sharma A. Nanotechnology: an emerging future trend in wastewater treatment with its innovative products and processes. Nanotechnology. 2012;1(2):1-8.

36. Mahmoodi V, Bastami TR, Ahmadpour A. Solar energy harvesting by magnetic-semiconductor nanoheterostructure in water treatment technology. Environmental Science and Pollution Research. 2018;25(9):8268-85. https://doi.org/10.1007/s11356-018-1224-y

37. Ahmadi M, Rahmani H, Takdastan A, Jaafarzadeh N, Mostoufi A. A novel catalytic process for degradation of bisphenol A from aqueous solutions: a synergistic effect of nano-Fe3O4@ Alg-Fe on O3/H2O2. Process safety and environmental protection. 2016;104:413-21. https://doi.org/10.1016/j.psep.2016.09.008

38. Chakhtouna H, Benzeid H, Zari N, Qaiss AEK, Bouhfid R. Recent progress on Ag/TiO(2) photocatalysts: photocatalytic and bactericidal behaviors. Environ Sci Pollut Res Int. 2021;28(33):44638-66. https://doi.org/10.1007/s11356-021-14996-y

39. Omrani E, Ahmadpour A, Heravi M, Bastami TR. Novel ZnTi LDH/h-BN nanocomposites for removal of two different organic contaminants: Simultaneous visible light photodegradation of Amaranth and Diazepam. Journal of Water Process Engineering. 2022;47:102581. https://doi.org/10.1016/j.jwpe.2022.102581

40. Cabrera L, Gutierrez S, Menendez N, Morales M, Herrasti P. Magnetite nanoparticles: electrochemical synthesis and characterization. Electrochimica Acta. 2008;53(8):3436-41. https://doi.org/10.1016/j.electacta.2007.12.006

41. Scherrer P. Bestimmung der inneren Struktur und der Größe von Kolloidteilchen mittels Röntgenstrahlen. Kolloidchemie Ein Lehrbuch: Springer; 1912. p. 387-409. https://doi.org/10.1007/978-3-662-33915-2_7

42. Saien J, Ojaghloo Z, Soleymani AR, Rasoulifard MH. Homogeneous and heterogeneous AOPs for rapid degradation of Triton X-100 in aqueous media via UV light, nano titania hydrogen peroxide and potassium persulfate. Chem Eng J. 2011;167(1):172-82. https://doi.org/10.1016/j.cej.2010.12.017

43. Souza R, Freitas T, Domingues F, Pezoti O, Ambrosio E, Ferrari-Lima A, Garcia J. Photocatalytic activity of TiO2, ZnO and Nb2O5 applied to degradation of textile wastewater. Journal of Photochemistry and Photobiology A: Chemistry. 2016;329. https://doi.org/10.1016/j.jphotochem.2016.06.013

44. Buddee S. Applications of TiO2 with energy in visible light region: Prince of Songkla University; 2015.

45. Serrà i Ramos A, Philippe L, Perreault F, Garcia-Segura S. Photocatalytic treatment of natural waters. Reality or hype? The case of cyanotoxins remediation. Water Research, 2020, vol 188, p 116543. 2020. https://doi.org/10.1016/j.watres.2020.116543

46. Curcó D, Giménez J, Addardak A, Cervera-March S, Esplugas S. Effects of radiation absorption and catalyst concentration on the photocatalytic degradation of pollutants. Catal Today. 2002;76(2-4):177-88. https://doi.org/10.1016/S0920-5861(02)00217-1

47. Bayarri B, Illana E, Curcó D, Giménez J, Esplugas S. Approach to TiO2-light interaction in heterogeneous photocatalysis. Water Sci Technol. 2007;55(12):147-51. https://doi.org/10.2166/wst.2007.394

48. Ghanbari F, Khatebasreh M, Mahdavianpour M, Lin K-YA. Oxidative removal of benzotriazole using peroxymonosulfate/ozone/ultrasound: Synergy, optimization, degradation intermediates and utilizing for real wastewater. Chemosphere. 2020;244:125326. https://doi.org/10.1016/j.chemosphere.2019.125326

49. Razani A, Abdullah AH, Fitrianto A, Yusof NA, Gaya UI. Sol-gel synthesis of Fe2O3-doped TiO2 photocatalyst for optimized photocatalytic degradation of 2, 4-dichlorophenoxyacetic acid. Oriental Journal of Chemistry. 2017;33(4):1959. https://doi.org/10.13005/ojc/330442

50. Li R, Jia Y, Bu N, Wu J, Zhen Q. Photocatalytic degradation of methyl blue using Fe2O3/TiO2 composite ceramics. Journal of Alloys and Compounds. 2015;643. https://doi.org/10.1016/j.jallcom.2015.03.266

51. Ambrus Z, Balázs N, Alapi T, Wittmann G, Sipos P, Dombi A, Mogyorósi K. Synthesis, structure and photocatalytic properties of Fe (III)-doped TiO2 prepared from TiCl3. Applied Catalysis B: Environmental. 2008;81(1-2):27-37. https://doi.org/10.1016/j.apcatb.2007.11.041

52. Rasouli K, Alamdari A, Sabbaghi S. Ultrasonic-assisted synthesis of α-Fe2O3@TiO2 photocatalyst: Optimization of effective factors in the fabrication of photocatalyst and removal of non-biodegradable cefixime via response surface methodology-central composite design. Separation and Purification Technology. 2023;307:122799. https://doi.org/10.1016/j.seppur.2022.122799

J. Water Environ. Nanotechnol., 9(1): 1-17 Winter 2024

17